Chapter-5

Deposition and Characterization of Yttrium oxide thin films deposited using $Y(thd)_3$ and $Y(tod)_3$ precursors

In this chapter, comparative study of Y_2O_3 thin films deposited by using two different precursors, $Y(thd)_3$ and $Y(tod)_3$ is reported. The octanedionate (tod) precursors are more volatile and this results in reduced carbon incorporation in deposited film as compared to when heptanedionate (thd) precursor is used. Comparative study is performed through characterizations results on films deposited using these two precursors under identical experimental conditions.

5.1 Introduction

As stated earlier in Chapter-1, deposition of Y_2O_3 thin films by using $Y(thd)_3$ precursor have been done by various groups. However, there are very few reports on deposition of Y_2O_3 thin films by using $Y(tod)_3$ precursor [**51**]. Niu et al. have reported deposition and characterization of Y_2O_3 thin films deposited by yttrium hexafluoroacetylacetonate [$Y(HFAA)_3$] and tris(2,2,6,6-tetramethyl-3,5-heptanedionate) yttrium [$Y(tmhd)_3$] using RF plasma CVD [**37**]. They have extensively studied effects on interface formation during deposition and post deposition annealing. Pasko et al. have earlier done a comparative study of heptanedionate (thd) and octanedionate (tod) precursors for deposition of hafnium oxide and zirconium oxide thin films by pulsed liquid injection MOCVD. They have reported amorphous phase deposition at a temperature of 500-550 °C while crystalline phase was formed at 600-750 °C. They have reported that tod precursors

evaporate without leaving any residue and lead to higher growth rate as compared to thd precursor. They found films deposited with tod precursors to be smooth and containing less carbon incorporation as compared to the thd precursor [**10**]. But there has been no such comparative study in case of yttrium oxide films deposited using (thd) and (tod) precursors by RF plasma enhanced MOCVD process under the influence of RF self bias on the substrates.

5.2 Experimental details for deposition of Y_2O_3 thin films by using $Y(thd)_3$ and $Y(tod)_3$ precursors

The schematic of deposition system is shown in **Figure-2.2** in chapter 2. The films were deposited by using two different precursors; $Y(thd)_3$ (film A) and $Y(tod)_3$ (film B) by RF plasma enhanced MOCVD. TGA plots for both the precursors are shown in **Figure 2.1** (**a** and **b**) in chapter 2. Silicon (100), quartz, tantalum and stainless steel substrates were used for deposition. The cleaning process of substrates has been mentioned in Chapter-2. After placing the cleaned substrates on the RF electrode, the chamber along with the precursor container and gas delivery lines are evacuated to a base pressure of 6×10^{-2} mbar pressure using a rotary vacuum pump. The delivery lines and precursor distributor ring (200 °C) are heated to avoid condensation of precursor in its path while the substrates are heated to a temperature of 350 °C with the help of programmable heater controller. Before deposition, the substrates are sputtered cleaned using plasma of argon gas (flow rate 5 sccm) at a substrate bias of -150 V for 20 minutes. The precursor container is gradually heated to a temperature of 200 °C. After sputtering, plasma of precursor vapors, oxygen (10 sccm) and argon (2 sccm) is generated and the substrate bias is adjusted to -75 V for deposition. The

deposition is carried for duration of 60 minutes. During the deposition of film A and film B, only the precursors used are different, all the other experimental parameters are kept same. The operating pressure during deposition for film A was ~ 3 x 10^{-1} mbar while for film B was ~ 4 x 10^{-1} mbar.

5.3 Characterization of Y_2O_3 thin films deposited by using $Y(thd)_3$ and $Y(tod)_3$ precursors

The deposited films are characterized by GIXRD, XPS, FTIR, spectroscopic ellipsometry, SEM and thickness measurement. GIXRD was carried out using a Cu K_α radiation source using Bruker D8 Discover model. The incident (grazing) angle was fixed at 1.8°. The scans were taken in 2θ range of 10°-90° with scan step of 0.02° per 3 second. XPS was done by VG make CLAM-2 model hemispherical analyzer with Mg K_α source (1253.6 eV). FTIR measurements were recorded in Far-IR region using Bruker Vertex 80V FTIR spectrometer configured with Mylar beam splitter and DTGS detectors at 4 cm^{-1} spectral resolution. An 11° reflection accessory was used for the measurements. Ellipsometric studies were carried out with a phase modulated spectroscopic ellipsometry unit (model UVSELTM 460 ISA JOBIN-YVON, SPEX) in the range 300-1200 nm. Thickness measurement was done using Veeco make Dektak 150 stylus profilometer. SEM analysis was done by using Carl Zeiss SEM (Supra 55). Characterization results obtained are as follows,

5.3.1 *Thickness measurement*

The thickness of film A is 0.33 µm while that of film B is 1.09 µm.

5.3.2 *Grazing Incidence X-ray diffraction*

The GIXRD patterns taken on the films are shown in **Figure 5.1**. The diffraction lines corresponding to (211), (222), (400), (440) and (622) reflections as indicated in JCPDF card No. 79-1716 do match well with the observed pattern for film A. This indicates deposition of Y_2O_3 with BCC structure for film A. Broad and diffused diffraction lines corresponding to (222), (440) and (622) reflections indicating deposition of BCC structure are also seen in case of film B. Diffraction lines are sharp and intense in case of film A while in case of film B the lines are broadened indicating formation of nanocrystalline phase.

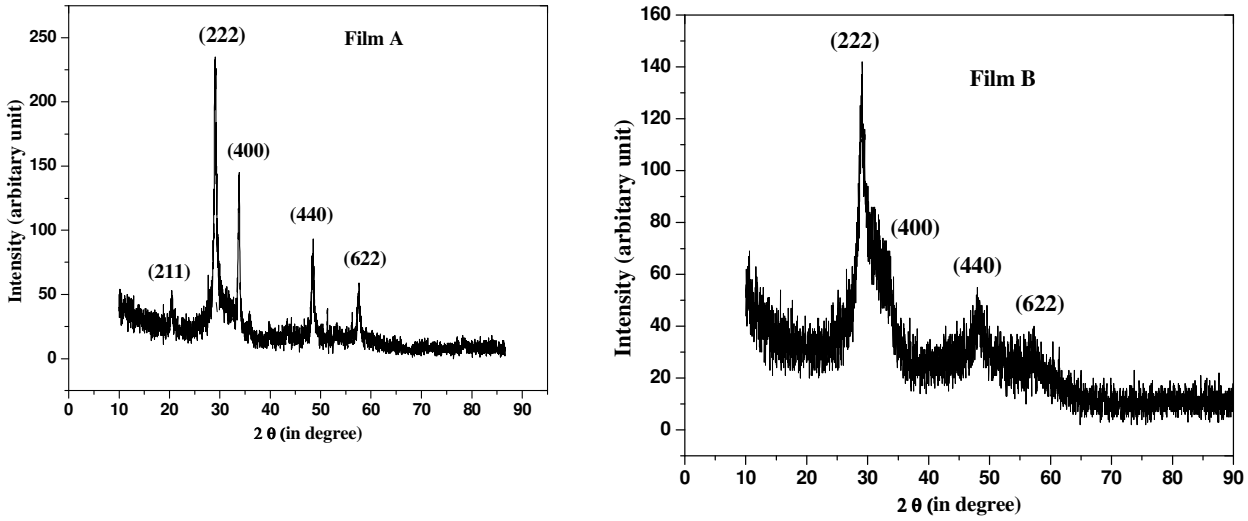

Figure 5.1: GIXRD patterns for films A and B

5.3.3 *X-ray Photoelectron Spectroscopy (XPS)*

The XPS scan was taken with pass energy of 22 eV. Peaks corresponding to Y 3*d* and O 1*s* are scanned in detail with 0.2 eV scan step. XPS Peak fit 4.1 program is used for

deconvolution of the peaks. The binding energy shifts were corrected using binding energy of physiadsorbed carbon at 284.6 eV as reference **[107]**.

Y 3*d* deconvoluted peaks for films A and B are shown in **Figure 5.2**. The Y 3*d* core level is getting split into doublet (Y $3d_{5/2}$ and Y $3d_{3/2}$) due to spin orbit coupling. The doublet has energy separation of 2.1 eV and Y $3d_{5/2}$ to Y $3d_{3/2}$ areal intensity ratio is 1.5 [**107**]. The Y 3*d* peak is deconvoluted with Gaussian: Lorentzian (G: L) ratio of 40 with FWHM of individual peaks in the range of 1.4-1.7 eV and chi-square (χ^2) value in the range of 0.7-2. Two different chemical environments are found for the yttrium atoms in both the films. Peak pair with binding energy at ~156.8 eV and ~158.8 eV correspond to stoichiometric yttrium oxide, peak pairs with binding energy at ~157.8 eV and ~160 eV could be either Y-OH or Y-OC bonds [**39**].

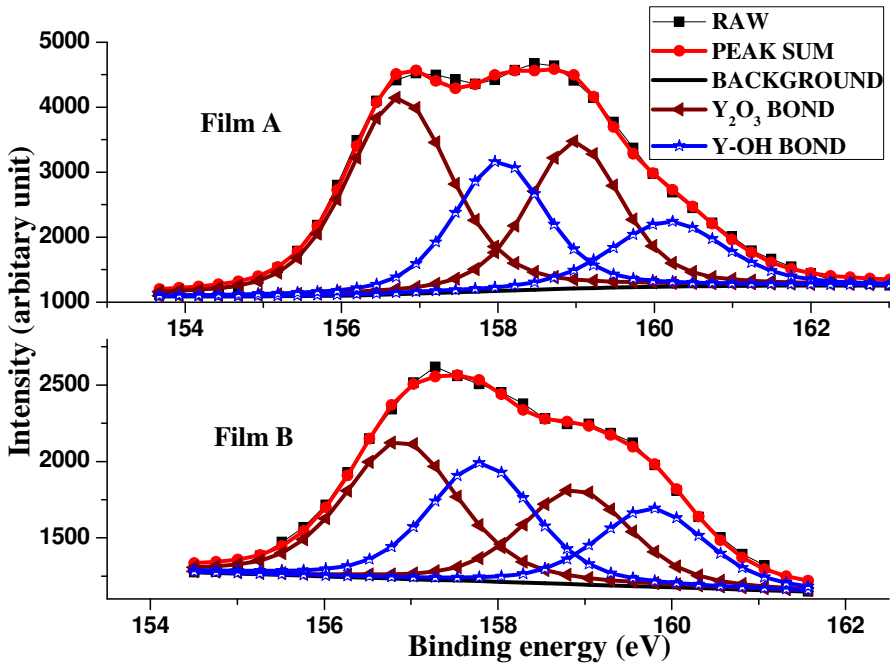

Figure 5.2: Detailed scan of Y 3*d* peak for films A and B

Deconvoluted O 1*s* peaks for both the films are shown in **Figure 5.3**. The O 1*s* peak is deconvoluted with Gaussian:Lorentzian (G:L) ratio of 40 with FWHM of individual peaks in the range of 1-1.8 eV and chi-square (χ^2) value in the range of 0.6-1.4. The O 1*s* peak for film A is deconvoluted into three sub peaks with binding energy, ~ 529.5 eV, ~ 530.5 eV and ~ 532eV corresponding to stoichiometric yttrium oxide, hydroxide (-OH) bond and C=O bond respectively while O1*s* peak for film B has three sub peaks at ~ 529.5 eV, ~ 530.5 eV and ~ 531 eV corresponding to stoichiometric yttrium oxide, -OH bond and O-C=O bond respectively [**120**].

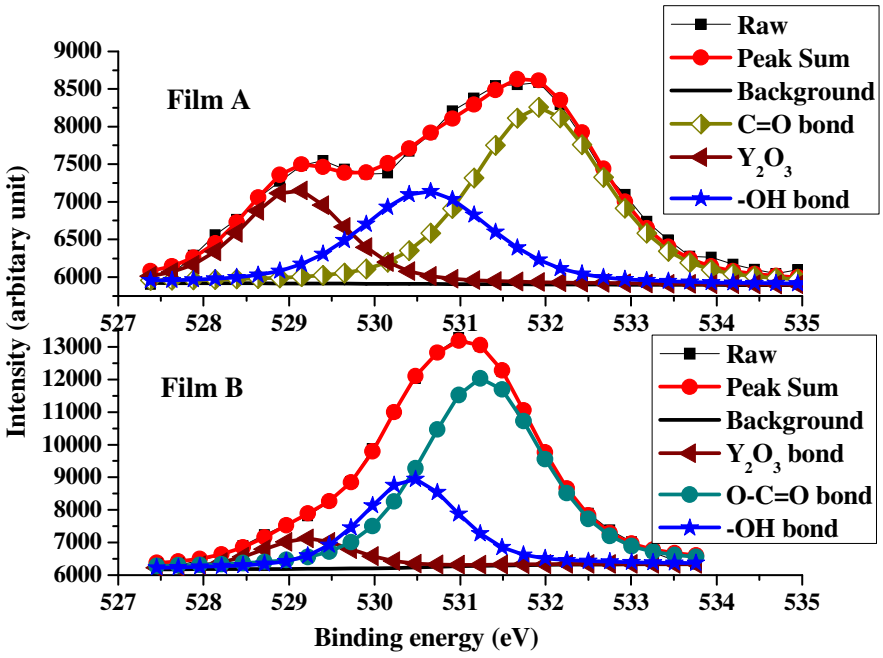

Figure 5.3: Detailed scan of O 1*s* peak for films A and B

5.3.4 *Infrared Spectroscopy*

The Far-IR reflectance spectra taken on the films are shown in the **Figure 5.4**.

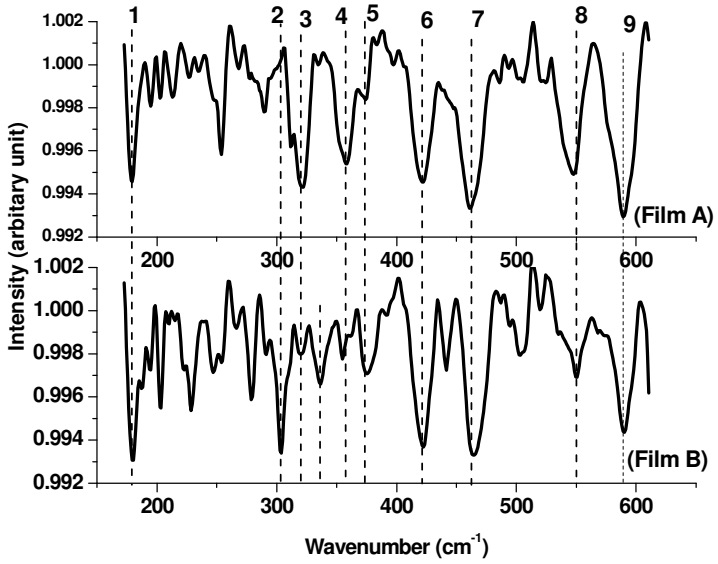

Figure 5.4: Far-IR reflectance spectrum for films A and B

The triplet at ~ 302 cm^{-1}, ~ 320 cm^{-1} and ~3 75 cm^{-1} indicating cubic Y_2O_3 structure is more clearly resolved for film B as compared to film A. Both the films show bands at ~178 cm^{-1}, ~ 358 cm^{-1}, ~ 420 cm^{-1}, ~ 462 cm^{-1}, ~ 560 cm^{-1} and ~ 582 cm^{-1} indicating cubic structure [**54, 108**].

5.3.5 *Spectroscopic Ellipsometry*

The variation of refractive index with wavelength in the range 300-1200 nm is shown in **Figure 5.5(a)**. The refractive index almost remains constant for both the films in the range of 600-1200 nm and as wavelength decreases below 600 nm, refractive index increases as reported in the literature [**43**]. Value of refractive index of film B is more than refractive index value of film A.

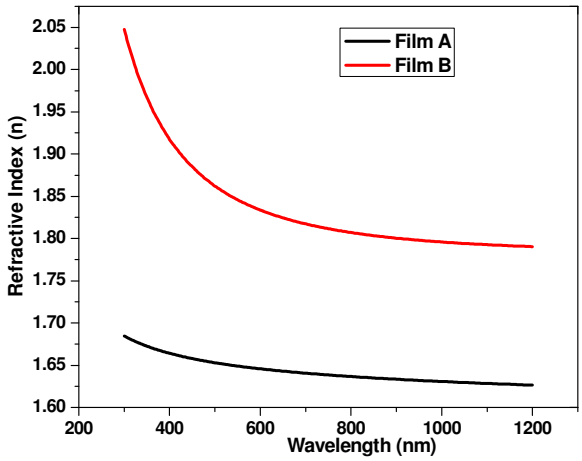

Figure 5.5(a): Variation of refractive index (n) for films A and B

The variation of extinction coefficient with wavelength in the range of 300-1200 nm is shown in the **Figure 5.5(b)**. Film B shows increased value of extinction coefficient as compared to film A. This indicates enhanced absorption in film B.

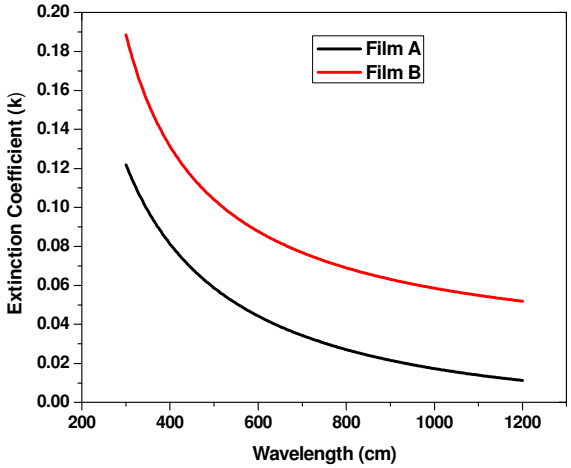

Figure 5.5(b): Variation of extinction coefficient (k) for films A and B

5.3.6 *Scanning electron microscopy*

The SEM images taken on the films A and B are shown in **Figure 5.6(a)** and **Figure 5.6(b)**. SEM images indicate formation of granular structure for both the films.

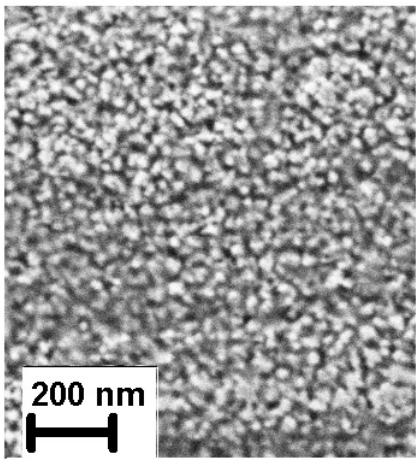

Figure 5.6(a): SEM image of film A

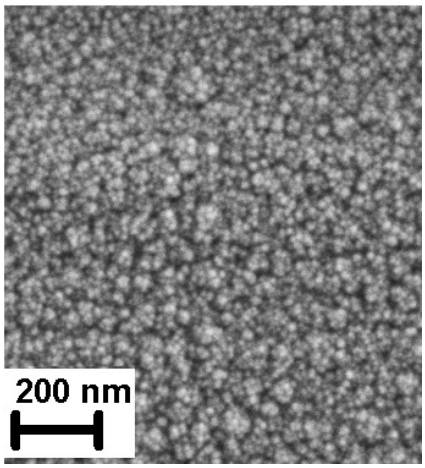

Figure 5.6(b): SEM image of film B

5.4 Discussion: Comparative study of properties of Y_2O_3 thin films deposited by using $Y(thd)_3$ and $Y(tod)_3$ precursors

It is seen that the thickness of film B is more than the thickness of film A. This is due to enhanced volatility of $Y(tod)_3$ precursor as compared to $Y(thd)_3$ precursor. This can be seen from TGA of precursors shown in **Figure 2.1** (**a** and **b**) in chapter-2**.** The enhanced volatility of tod precursors was reported earlier by Pasko and co-workers in case of $Hf(tod)_4$ and $Zr(tod)_4$ precursors stating tod precursors to be less thermally robust then the corresponding thd precursors [**10**]. In case of $Y(tod)_3$ hydrogen has been substituted by a methyl radical so enhanced shielding effect increases the volatility [**8**]. From the TGA plots it is seen that, for the $Y(thd)_3$ precursor at temperature of 200 °C, mass loss is approximately

40 % while for the $Y(tod)_3$ precursor at 200 °C, the mass loss is approximately 67 %. At 300 °C temperature, the mass loss for $Y(thd)_3$ precursor is 59 % while that for $Y(tod)_3$ precursor increases to 89 %.

From GIXRD patterns it is seen that film A has polycrystalline nature with BCC structure. Though peaks have broadened in case of film B, the GIXRD pattern seen in case of film B is also consistent with that of cubic yttrium oxide. The broad GIXRD peaks and high background of diffraction spectrum indicate that the film B has poor crystallinity as earlier reported by Kokuoz et al. [**111**]. This indicates that particle size in case of film B has decreased and there is formation of nanocrystalline structure. The broadened GIXRD peaks in case of film B may be due to increase in deposition pressure [**22**]. Both the films show textured growth along (111) direction. As yttrium oxide has bixbyite structure, (111) plane has minimum surface energy and hence preferred growth direction is along (111) [**43**]. Earlier Pasko et al. have obtained amorphous films of ZrO_2 and HfO_2 using thd and tod precursor at temperature of 550 °C by pulsed liquid injection method [**10**]. In the current work, it is seen that crystalline film deposition of Y_2O_3 is possible even at temperature of 350 °C due to high internal energy of plasma state during deposition.

Far-IR reflectance spectra confirm deposition of cubic Y_2O_3 structure in both the films. The triplet at ~ 302 cm^{-1}, ~ 320 cm^{-1} and ~ 375 cm^{-1} is more clearly resolved in case of film B than film A as thickness of film B is more than film A. The other bands ~178 cm^{-1}, ~ 358 cm^{-1}, ~ 420 cm^{-1}, ~ 462 cm^{-1}, ~ 560 cm^{-1} and ~ 582 cm^{-1} indicating cubic structure are present in both the films [**54, 108**]. SEM images for both the films indicate granular structure for both the films. This is in agreement with the GIXRD and FTIR results, confirming that film B is nanocrystalline and not amorphous in nature.

Yttrium oxide is hygroscopic in nature; hence it has a tendency to absorb moisture. The moisture further reacts with atmospheric carbon to form carbonate and hydro carbonate bonds [**46**]. The films were not sputtered prior to XPS scan hence surface adsorbed moisture and carbon species are present. Hence semi quantitative analysis is done by considering only the Y 3*d* peak [**48**]. Semi quantitative analyses from Y 3*d* peak indicate higher percentage of Y-OC bonds (44 %) on the surface of film B as compared to film A (36 %) while the amount of stoichiometric Y_2O_3 is higher in film A (64 %) as compared to film B (56 %). The O 1*s* peak deconvolution for film A shows that in addition to yttrium oxide there are hydroxide and carbonate bonds present at the surface of the film. The O 1*s* peak deconvolution for film B is dominated by the presence of carbonate bonds.

Reason for increase in carbon adsorption in case of film B is its nanocrystalline structure. Nanostructures have enhanced surface area as compared to their volume leading to greater amount of adsorption of atmospheric gases such as moisture and carbon dioxide [**111**].

Ramana et al. have reported that value of refractive index (n) and extinction coefficient (k) is also enhanced due to formation of dense network of nanocrystals [**65]**. This can be seen from the ellipsometry measurements of film B. Both refractive index (n) and extinction coefficient (k) values have increased in case of film B. The increase in (n) shows film B has higher density. Although film B shows higher amount of adsorbed moisture and carbon species on the surface its refractive index is not affected as earlier reported by Kokuoz and co-workers [**111**]. Comparative decrease in refractive index in case of film A indicates that film A is not as dense as film B. Although film A has good crystallinity, the density of film B is higher due to formation of nanocrystalline phase. Kim et al. had earlier

reported that structural changes dominate the stoichiometric effects in deciding the refractive index of Y_2O_3 [**110**]. The enhancement of refractive index for nanocrystalline Y_2O_3 film as compared to well crystallized film was also observed in our earlier study reported in chapter 3.

Conclusion

Investigations reported here indicate that both the films deposited using $Y(thd)_3$ and $Y(tod)_3$ have BCC structure. Higher deposition rate can be achieved using $Y(tod)_3$ precursor. There is formation of nanocrystalline structure for the film deposited using $Y(tod)_3$ precursor. The film deposited using $Y(tod)_3$ precursor shows enhanced refractive index indicating higher density of the film.